Prediction of long-term dynamics from transients

Joachim Holzfuss
Institut für Angewandte Physik, TU Darmstadt, Schloßgartenstr. 7, 64289 Darmstadt, Germany
(Received 13 August 2003; revised manuscript received 4 August 2004; published 13 January 2005)

Existing methods of time series analysis of nonlinear dynamical systems deal with the dynamics on single (strange) attractors. We extend this method for systems that can be externally manipulated. We interact with a previously unknown system by perturbing it randomly and recording the responses. By following transients for a short time and approximating the global flow, we can predict the final long-term dynamics, including coexisting multistable, chaotic, or periodic dynamics. Also the localization of basins of attraction is possible, enabling the selection or control of the type of final dynamics. Numerical and experimental examples of driven nonlinear oscillators are given.

DOI: 10.1103/PhysRevE.71.016214 PACS number(s): 05.45.Tp, 47.52.+j

I. INTRODUCTION

Time-series analysis of nonlinear dynamical systems [1] is inspired greatly by the time-shift embedding procedure [2–4]. Together with the concept of attractors governing the system dynamics, the construction of trajectories in an equivalent state space opens a wide field for the analysis of experiment data. Dynamical invariants, such as fractal dimensions [5,6], Lyapunov exponents [7–9], and dynamical entropies [10], have been computed from data and resulted in deeper insight into the nature of the processes generating the data. The basis of the embedding procedure is to record the time dependence of one observable or coordinate and to construct trajectories in an equivalent state space with the help of time-shifted values of the same observable [11,12]. If the system behaves chaotically or "explores" the state space to a large extent, dynamical measures can be calculated as the neighborhood of trajectories is visible by the recurrent nonlinear dynamics on the strange attractor. Only a small part of the state space is visible, if only a periodic motion is present. If the overall system dynamics has multiple stable attractors, then they cannot be found from a single trajectory.

We propose to interact with the system and record its response. In this way the neighborhood of trajectories can be explored and the information can be used to predict the type of future dynamics, starting at a specified initial condition or after a specific perturbation. To accomplish this, the system is randomly perturbed and some small time series are taken from one observable. The perturbations are understood not as additive random noise on an observable, but as a change in the dynamics, e.g., by random selection of the systems state, a sudden change in system parameters [13,14], or by a temporary coupling to another system. From the small time samples, trajectories are constructed using time-shifts. The global flow is approximated using the recorded time evolved values of the initial conditions. It can be applied to any interesting starting point. Basins of attraction can be measured and predicted and also the final wave forms.

II. NUMERICAL PROCEDURE

The global flow

$$\Psi:\mathbb{R}^m \to \mathbb{R}^m, \quad \mathbf{x} \mapsto \Psi^{\Delta t}(\mathbf{x}) \tag{1}$$

of a system maps an initial state $\mathbf{x}$ to its time evolved value. Sequentially applying the flow generates a system trajectory. If only one coordinate $x(t)$ is measured, a theorem [4] guarantees that when using proper time-shifted values of one coordinate the resulting attractor is an embedding of the original one. This holds in all generic cases provided the embedding dimension is larger than twice the dimension of the set in the original state space.

New vectors are constructed

$$\mathbf{y} = \{x(0), x(T), \ldots, x((n-1)T)\}. \tag{2}$$

Their time-evolved value is given by applying the flow Φ in this space

$$\Phi:\mathbb{R}^n \to \mathbb{R}^n, \quad \mathbf{y} \mapsto \Phi^{\Delta t}(\mathbf{y}). \tag{3}$$

Our extension of the standard method is that we do not merely follow the dynamics of the unperturbed system, hence, mapping the embedded trajectory on some attractor, but investigate the time evolution of different random points in the state space. This flow Φ is approximated by a function $f:\mathbb{R}^n \to \mathbb{R}^n$ by averaging over the time evolution of a set of initial conditions $\{\mathbf{y}_k\}$ (data vectors). For this approximation, radial basis functions [15–19] are used;

$$\Phi^{\Delta t}(\mathbf{y}_k) \approx f(\mathbf{y}_k) = \sum_{l=1}^{N} \mathbf{c}_l \sigma(\mathbf{y}_k, \mathbf{z}_l), \quad \mathbf{c}_l \in \mathbb{R}^n \tag{4}$$

$$\sigma(\mathbf{y}_k, \mathbf{z}_l) = \sqrt{r^2 + \|\mathbf{y}_k - \mathbf{z}_l\|^2} \quad r \in \mathbb{R}^+ \tag{5}$$

σ are radial basis functions and $\{\mathbf{z}_l\}$ is a set of data vectors (called centers). In general, the data vectors can be the same as the centers, but may be random subsets of all available data vectors [15], as done in the numerical examples. r is a stiffness factor, whose value is taken to be the average squared euclidian norm in Eq. (5); a choice which resulted in

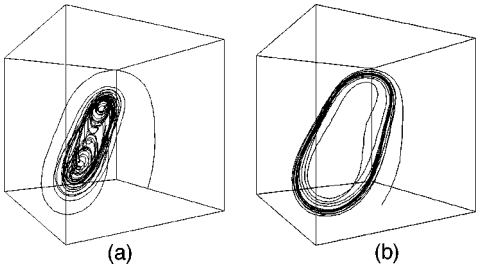

FIG. 1. Two transients of the Duffing oscillator evolving into their final coexisting attractors (a) chaotic, (b) periodic, in time-shift coordinate state space of the x coordinate.

the best predictive abilities (see the Appendix). The coefficients $\mathbf{c}_l$ have to be determined by solving the linear equation (4) for each dimension. Knowing the approximated global flow f, the time evolution of any initial vector can be traced by iterated mapping.

III. NUMERICAL EXAMPLE

The forced Duffing oscillator is used as an example. Parameters were taken such that two attractors are coexisting

$$\ddot{x} + d\dot{x} - x + x^3 = a\cos(\omega t), \tag{6}$$

with $d=0.2$, $a=1$, $\omega=1.7$. Figure 1 shows two different transients visualizing the evolution of the system state to the final dynamics being either governed by a chaotic or a periodic attractor. The state space shown is the time-shift coordinate state space generated from the time evolution of the x coordinate of Eq. (6). The integration time step (sampling rate) is $t_s \approx 1/25$ points per driving period. The time delay for the attractor construction is $4t_s$. This not very critical value can be determined with information theoretic measures [10,20], geometric considerations [21,22], or very roughly from an autocorrelation.

For the approximation of the global flow an embedding dimension of $n=5$ is appropriate (see the Appendix). The starting points of the transients are taken from a regular $16 \times 16 \times 10$ grid in the $(x, \dot{x}, \phi)$ space, where $[-4.5, 4.875]$ was the range of x and $\dot{x}$ values (the gray square in Fig. 2) and $[0, 2\pi]$ for $\phi = \omega t \bmod 2\pi$. To accelerate the calculation, random subsets of the transient trajectories have been chosen. The number of centers $\mathbf{z}_l$ is 1000 and the number of data vectors $\mathbf{y}_k$ is 400. The evolution time $\Delta t = 1 t_s$.

Figure 2(a) shows the basins of attraction for the coexisting periodic and chaotic attractor of data generated from Eq. (6). The initial conditions for the transients are taken from a Poincaré plane at a certain driving phase. In Fig. 3, the action of the flow on these initial vectors is seen. From the first segments of the x coordinate of the time evolution of initial vectors from the Poincaré plane a three-dimensional time-shift embedding is done to visualize the action of the flow of the system together with the final attractors.

Figure 2(b) shows the basins calculated by iterated mapping using the approximated flow. The $(x, \dot{x})$ coordinates of the data vectors for the approximation of the flow are located within the gray square. It is seen that by iterated mapping of

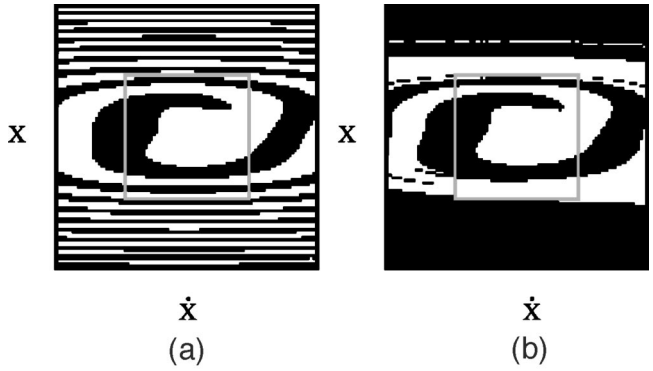

FIG. 2. Basins of attraction of two coexisting attractors of the Duffing oscillator for 100×100 initial conditions. (a) Direct calculation via the differential equation. (b) Calculation via the approximated global flow. Black: periodic; white: chaotic. The gray square in the middle shows the region used for the approximation.

the time evolution of the initial conditions the final attractors and the basin boundaries can be found remarkably well. Also, mapping initial vectors from the outside of the gray region vectors seems to be possible, though not from every direction. This may be due to the finite amount of data used for the approximation.

IV. EXPERIMENT

A simple driven nonlinear RLC circuit [23,24] is used for an experimental demonstration of the method. It consists of a resistor ($R=200\ \Omega$), an inductivity ($L=4.1$ mH), and a diode with voltage-dependent capacity (Type 1N4007) connected in series. It is driven by a sine voltage of 55.824 kHz and 2.2 V. These parameters are set such that there are two coexisting period-1 attractors, one with a larger and one with a smaller maximum amplitude. This is happening in the bista-

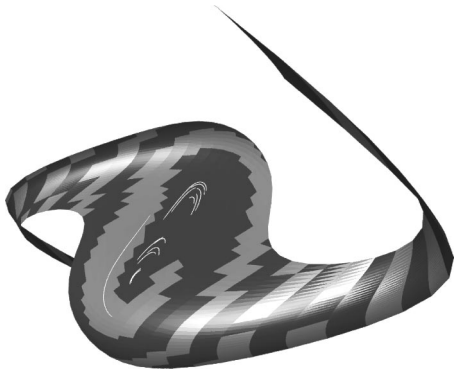

FIG. 3. Initial conditions lying in a Poincaré plane ($t=1.75$) of the Duffing oscillator [Eq. (6)] and their time evolution are recorded. The first short time segments of the x coordinate are used to construct an image of this plane. The axis are spanned by the time-shift coordinate state space of the x coordinate. The two coexisting stable attractors are shown crossing the plane. The tiles are color coded with respect to the final attractor. The Poincaré plane in the original state space is the same as in Fig. 2(a). It is deformed by the action of the flow.

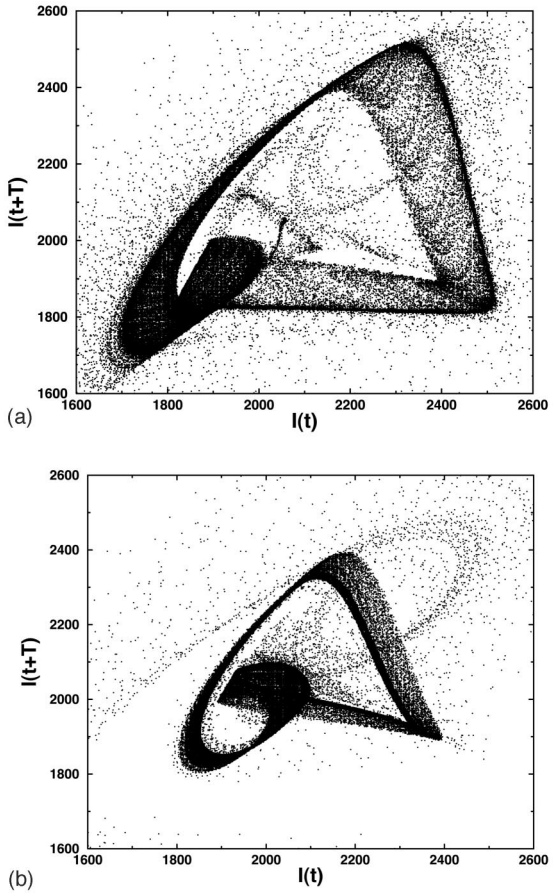

FIG. 4. Transients of the RLC oscillator experiment with parameters set such that two coexisting stable periodic attractors are present. The dynamics is shown in the time-shift coordinate state space of the measured current. The circuit has been randomly perturbed, and the current has been measured after the perturbations have been switched off. The transients shown have been sorted for their final dynamics. (a) Transients finally approaching a "big" attractor. (b) Transients for the "small" attractor. The attractors themselves are located the most dense part of the plots.

bility region (hysteresis) of the main resonance of the oscillator, which, due to the soft (Toda) potential of the oscillator, is shifted heavily toward lower frequencies. The linear resonance frequency of the circuit is at ≈270 kHz. The current through the circuit is measured by sampling the voltage over the resistor with 2 MHz sampling frequency. This corresponds to a little less than 36 samples per driving period.

In order to produce transient dynamics, the amplitude of the driving sine-wave generator is amplitude modulated with a slow frequency (≈147 Hz) for about 0.6 ms gating time. The amplitude modulation generates quasirandom initial conditions. Care is taken not to produce rational ratios between the involved frequencies. The start of the gate of the modulation is not phase locked to the driving signal. The recording of transients starts when the gate pulse (and with it the modulation) falls to zero. This way the unperturbed transient dynamics is recorded of 5000 trajectories with the length of 176 samples.

Figure 4 shows the transient trajectories in time-shift state space. They are sorted by the final attractor they are approaching. It is possible to appreciate the complex structure of the basins for the two periodic attractors.

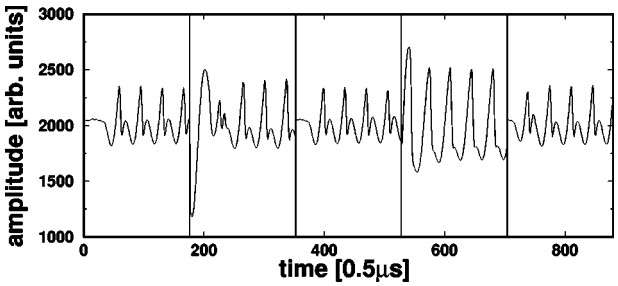

FIG. 5. Time series of the current of the RLC circuit. Five different transients are shown. The fourth transient is reaching the big periodic attractor, while the other ones approach the small one.

Figure 5 shows some examples of the transient time series involved. The time series are taken after the perturbation has been switched off. The circuit is driven freely with a pure sine wave and the current oscillations are approaching their respective final wave forms.

To predict a final current oscillation and its wave form, the global flow is approximated from a random collection of 400 data vectors and 2000 random centers. The embedding dimension is $n=6$ with a time-shift value of $T=2t_s$ as obtained by the method described in the Appendix. The evolution time taken is $\Delta t=1t_s$. From the recorded trajectories only the first time segment of length $(n-1)T+\Delta t=11t_s$ is used for the calculation.

When the flow is approximated, a random initial data vector is chosen and mapped with the approximated function f. Using this predicted current value and the past values, a vector is constructed and the whole procedure is iterated until a final oscillation wave form is reached. Figure 6 shows 2 examples of predicted currents from random initial snippets. Both periodic orbits are shown; their period equals that of the driving. The final wave forms are the "big" and the "small" ones, which are the two current wave forms present in the system (see Fig. 5).

V. DISCUSSION

With the described method of embedding short-time transients to approximate the global flow, the prediction of future dynamics is possible. If a system is multistable, then the

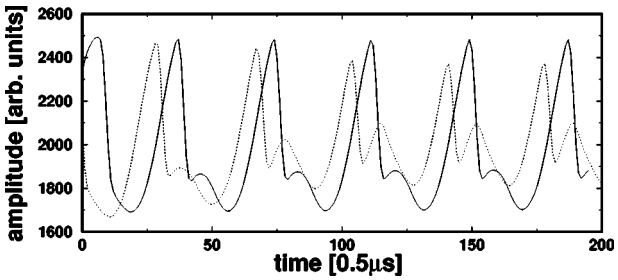

FIG. 6. Predicted current starting from two different initial conditions. One transient is approaching the big attractor, while the other one approaches the small periodic attractor.

basins of attraction can be predicted and the final dynamics of a single transient can be qualified. Also forecasts for initial points from the "outside" seem possible. For chaotic time series, short-term predictions can be made, also dynamical invariants can be computed from predicted data. In case of periodic motions, the final wave form is predicted.

Information can be retrieved by interaction with the system with perturbations and exploring the neighborhood of a trajectory. The tangent space can be calculated by differentiation of the function f, and the stability can be quantified by calculating eigenvectors and -values (e.g., a stable periodically running process can be randomly perturbed to probe its stability). The described method may also be of interest in combination with the control of trajectories on unstable periodic orbits [27]. As the tangent space information needed for the control is extracted by linearizing the flow, even the stabilization of perturbed and only weakly stable periodic motions can be achieved by mapping of the most stable directions leading to regular behavior. The extraction of information about coexisting dynamics is limited by the fact that random initial conditions used for the approximation cover the interesting parts of the state space. Appropriate experimental mechanisms have to be employed to accomplish this. In a situation of a very complex basin structure with a multitude of coexisting attractors, the method of tracking initial orbits may be numerically unfeasable. The procedures for the choice of time-shifts and embedding dimension follow much the same strategies as with conventional embedding. The amount of state space occupied by all transients after perturbation shrinks to the size of the attractor as time evolves. The embedding dimension should be increased to a value between the one suitable for the final attractor [28] and the one appropriate for the full dimension of the perturbed system. The latter one can be small for simple oscillators or very large when dealing with, e.g., time-delay feedback systems. When transients die out quickly the embedding dimension can be set closer to the lower bound. In the Appendix it is shown with the example of the duffing oscillator, that with increasing embedding dimension the prediction errors get smaller, saturate at an optimal value, and get worse again on further increase.

The approximation of the global flow is not limited to radial basis functions or a special choice of one despite of their good approximation properties. The approximation of polynomials or any other adapted function by least-squares methods or genetic algorithms is possible. Their numerical stability concerning iteration properties has to be determined though. Data-driven determination of the true system equations of periodic (and also chaotic) processes [25,26], which would never be one-to-one without further knowledge, seems possible.

ACKNOWLEDGMENT

Part of this work has been sponsored by the SFB 185 Nichtlineare Dynamik of the DFG.

APPENDIX: DETERMINATION OF EMBEDDING AND RECONSTRUCTION PARAMETERS

The proposed method relies on the embedding procedure [Eq. (2)]. There, an embedding dimension n and a time-shift T are used to construct new vectors. We have fixed their values by determination of the maximum of the signal-to-noise ratio (SNR) of the predicted values. The SNR in dB is defined as

$$\mathrm{SNR} = 20 \log_{10} \frac{\Delta y_n}{\Delta(\Phi_n^{\Delta t}(\mathbf{y}) - f_n(\mathbf{y}))}, \tag{A1}$$

which calculates the ratio of standard deviations of the time series to the errors of the nth predicted component, n being the embedding dimension. The SNR is a scaled logarithmic inverse of the normalized prediction error [29], 0 if the root-mean square of the error values equals that of the data points, and large for good predictions [15,30]. For the numerical data of Figs. 1–3, the time evolution of all used 2560 initial conditions of the forced duffing oscillator, the SNR is shown in Fig. 7. The maximum SNR is circled among various values obtained for different time-shifts T and embedding dimensions n. The optimal value coincides with the value found for data taken when the system dynamics is running on the single chaotic attractor. It shows, that the dynamics collapses fast to the dynamics on the respective attractor. This might not always be the case. If transients from coexisting periodic attractors are considered, then the embedding

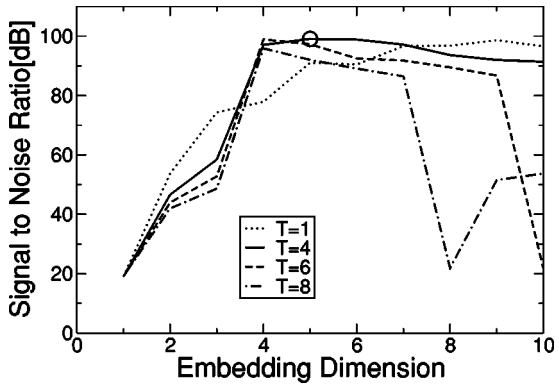

FIG. 7. Signal-to-noise ratio as a function of embedding dimension for various values of the time-shift T. The best approximation of all data points (see circle) is determined for the numerical example of the duffing oscillator.

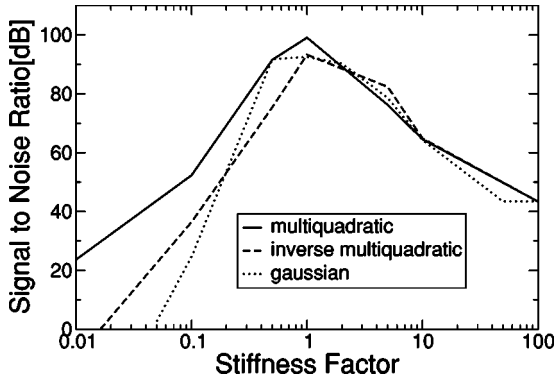

FIG. 8. Signal-to-noise ratio as a function of the stiffness coefficient for various types of radial basis functions. The optimal embedding parameters determined in Fig. 7 have been taken.

dimension has to be higher than the one required for the periodic attractors to unfold the system dynamics (e.g., in open systems after a perturbation the system dynamics may run in a very high-dimensional space, where the embedding dimension has to be considerably higher than that of the final attractor). Calculating the SNR is a method to find and justify the embedding parameters.

To evaluate the dependence on different types of radial basis functions (RBFs) and their parameters, the SNR is calculated for the multiquadratic RBF [Eq. (5)], the inverse multiquadratic RBF σ^{-1} and a Gaussian RBF $\sigma(\mathbf{y}_k, \mathbf{z}_l) = \exp(-\|\mathbf{y}_k - \mathbf{z}_l\|^2 / r^2)$. The stiffness parameter r is normalized to the average squared norm of the differences of data vectors $\mathbf{y}$ and centers $\mathbf{z}$. It is seen in Fig. 8 with the data of the numerical example, that the multiquadratic RBF with a stiffness factor $r=1$ gives the highest SNR for the predicted values. Therefore, these values have been taken in the further calculations.

[1] H. Kantz and T. Schreiber, *Nonlinear Time Series Analysis* (Cambridge University Press, Cambridge, England, 1997).

[2] F. Takens, in *Dynamical Systems and Turbulence*, edited by D. A. Rand and L. S. Young, Lecture Notes in Mathematics Vol. 898 (Springer-Verlag, Berlin, 1981), pp. 366–381.

[3] N. H. Packard, J. P. Crutchfield, J. D. Farmer, and R. S. Shaw, Phys. Rev. Lett. **45**, 712 (1980).

[4] T. Sauer, J. A. Yorke, and M. Casdagli, J. Stat. Phys. **65**, 579 (1991).

[5] P. Grassberger and I. Procaccia, Phys. Rev. Lett. **50**, 346 (1983).

[6] W. Lauterborn and J. Holzfuss, Phys. Lett. A **115**, 369 (1986).

[7] J. Holzfuss and W. Lauterborn, Phys. Rev. A **39**, 2146 (1989).

[8] J. Holzfuss and U. Parlitz, in *Lyapunov Exponents*, edited by L. Arnold, H. Crauel, and J.-P. Eckmann, Lecture Notes in Mathematics Vol. 1486 (Springer, Berlin, 1991), pp. 263–270.

[9] H. Herzel, J. Holzfuss, Z. Kowalik, B. Pompe, and R. Reuter, in *Nonlinear Analysis of Physiological Data*, edited by H. Kantz, J. Kurths, and G. Mayer-Kress (Springer, Berlin, 1998), pp. 325–344.

[10] A. M. Fraser and H. L. Swinney, Phys. Rev. A **33**, 1134 (1986).

[11] R. Hegger, H. Kantz, L. Matassini, and T. Schreiber, Phys. Rev. Lett. **84**, 4092 (2000).

[12] U. Parlitz, R. Zöller, J. Holzfuss, and W. Lauterborn, Int. J. Bifurcation Chaos Appl. Sci. Eng. **4**, 1715 (1994).

[13] D. Coles, J. Fluid Mech. **21**, 385 (1965).

[14] J. E. Burkhalter and E. L. Koschmieder, Phys. Fluids **17**, 1929 (1974).

[15] J. Holzfuss and J. B. Kadtke, Int. J. Bifurcation Chaos Appl. Sci. Eng. **3**, 589 (1993).

[16] D. S. Broomhead and D. Lowe, Complex Syst. **2**, 321 (1988).

[17] M. Casdagli, Physica D **35**, 335 (1989).

[18] R. Franke, Math. Comput. **38**, 181 (1982).

[19] S. Rippa, Adv. Comput. Math. **11**, 193 (1999).

[20] O. Göhrs and J. Holzfuss, in *Stochastic and Chaotic Dynamics in the Lakes: STOCHAOS*, edited by David S. Broomhead, Elena A. Luchinskaya, Peter V. E. McClintock, and Tom Mullin, AIP Conf. Proc. No. 502 (AIP, Melville, NY, 2000), pp. 668–673.

[21] Th. Buzug, T. Reimers, and G. Pfister, Europhys. Lett. **13**, 605 (1990).

[22] W. Liebert, K. Pawelzik, and H. G. Schuster, Europhys. Lett. **14**, 521 (1991).

[23] P. S. Linsay, Phys. Rev. Lett. **47**, 1349 (1981).

[24] C. D. Jeffries, Phys. Scr. **T9**, 11 (1985).

[25] J. Cremers and A. Hübler, Z. Naturforsch., A: Phys. Sci. **42**, 797 (1987).

[26] J. Crutchfield and B. MacNamara, Complex Syst. **1**, 417 (1987).

[27] E. Ott, C. Grebogi, and J. A. Yorke, Phys. Rev. Lett. **64**, 1196 (1990).

[28] T. Sauer and J. A. Yorke, Int. J. Bifurcation Chaos Appl. Sci. Eng. **3**, 737 (1993).

[29] J. D. Farmer and J. J. Sidorowich, Phys. Rev. Lett. **59**, 845 (1987).

[30] T. Sauer, Physica D **58**, 193 (1992).